Vision Research 164 (2019) 83–93

Contents lists available at ScienceDirect

Vision Research

journal homepage: www.elsevier.com/locate/visres

The melanopsin-directed white noise electroretinogram (wnERG)

Prakash Adhikari[a,b], Andrew J. Zele[a,b], Dingcai Cao[c], Jan Kremers[d], Beatrix Feigl[a,e,f,*]

[a] Visual Science and Medical Retina Laboratories, Institute of Health and Biomedical Innovation, Queensland University of Technology (QUT), Brisbane, QLD 4059, Australia
[b] School of Optometry and Vision Science, Queensland University of Technology (QUT), Brisbane, QLD 4059, Australia
[c] Visual Perception Laboratory, Department of Ophthalmology and Visual Sciences, University of Illinois at Chicago, Chicago, IL, USA
[d] Laboratory for Retinal Physiology, Department of Ophthalmology, University Hospital Erlangen, Erlangen, Germany
[e] School of Biomedical Sciences, Queensland University of Technology (QUT), Brisbane, QLD 4059, Australia
[f] Queensland Eye Institute, Brisbane, Australia

ARTICLE INFO

Keywords:
Electroretinogram
Melanopsin
Silent substitution
White noise electroretinogram (wnERG)

ABSTRACT

The white noise electroretinogram (wnERG) provides a measure of the impulse response function under conditions of retinal equilibrium; it is yet to be determined how the electrical response generated by melanopsin ganglion cell photoreception is expressed in the impulse response. To this end, we recorded the human wnERG to continuous temporal white noise (TWN) stimuli that were melanopsin-directed (rod and cone silent) or cone-directed (rod and melanopsin silent). The impulse response of the electroretinogram was derived by cross-correlating the TWN stimulus with the wnERG response. We observed that the LMS-cone directed wnERG contained the expected N1 wave (24.1 ± 2.4 ms; mean ± SEM) and P1 wave (49.7 ± 1.8 ms). Melanopsin-directed stimuli produced a unique wnERG with a slower negative deflection (N_m) at 62.9 ± 3.3 ms followed by a positive deflection (P_m) at 126.3 ± 5.1 ms. Additional experiments indicated this melanopsin-directed wnERG response was not due to cone intrusion. The N_m and N_mP_m amplitudes increased with illuminance (32,000–80,000 Td; no rod intrusion) and melanopsin contrast (10–36% Michelson contrast). As there are known pathways connecting melanopsin cells to the outer retina, we then measured the wnERG to combined melanopsin and cone-directed stimuli to quantify melanopsin interactions with cone signalling. With the combined stimuli, the N1P1 amplitudes were suppressed by ~59%, which may be a result of a destructive interference between the positive (P1) and negative (N_m) waves generated by the cone and melanopsin pathways. We conclude that the human wnERG to melanopsin-directed stimuli may reflect the combined response of intra-retinal melanopsin pathways, independent of rod and cone photoreception.

1. Introduction

In rodents and primates, melanopsin-expressing intrinsically photosensitive Retinal Ganglion Cells (ipRGCs) mediate photoreception independent of conventional rod and cone photoreceptors (Berson, Dunn, & Takao, 2002; Dacey et al., 2005; Gamlin et al., 2007; Grünert, Jusuf, Lee, & Nguyen, 2011; Lucas et al., 2003; Nasir-Ahmad, Lee, Martin, & Grünert, 2019) to regulate image forming (Cao, Chang, & Gai, 2018; Cao, Nicandro, & Barrionuevo, 2015; Horiguchi, Winawer, Dougherty, & Wandell, 2013; Spitschan et al., 2017; Zele, Adhikari, Cao, & Feigl, 2019b; Zele, Adhikari, Feigl, & Cao, 2018; Zele, Feigl, Adhikari, Maynard, & Cao, 2018) as well as non-image forming visual functions (Adhikari, Zele, & Feigl, 2015; Berson et al., 2002; Gamlin et al., 2007; Gooley et al., 2012; Kelbsch et al., 2019; Zele, Adhikari, Cao, & Feigl, 2019a). Rod and cone stimulations produce characteristic waveforms in the human flash electroretinogram (ERG) with a typical negative deflection followed by a positive deflection (Brown, 1968; Einthoven & Jolly, 1908; Friedburg, Allen, Mason, & Lamb, 2004; Friedburg, Thomas, & Lamb, 2001; Granit, 1933; Heckenlively, Arden, Nusinowitz, Holder, & Bach, 2006; McCulloch et al., 2015). There are a few studies of the melanopsin contribution to the light-adapted photopic flash ERG, with evidence that the response is dependent on the recording conditions (Allen & Lucas, 2016; Fukuda, Higuchi, Yasukouchi, & Morita, 2012). In mice, there is no response to a melanopsin-directed flash ERG under conditions of silent substitution (Allen & Lucas, 2016). However, in humans, using similar colorimetric techniques to the study in mice, but with higher adaptation levels and longer flash duration and recording epochs, the melanopsin

* Corresponding author at: Visual Science and Medical Retina Laboratories, Institute of Health and Biomedical Innovation, Queensland University of Technology (QUT), Brisbane, QLD 4059, Australia.
E-mail address: b.feigl@qut.edu.au (B. Feigl).

https://doi.org/10.1016/j.visres.2019.08.007
Received 26 November 2018; Received in revised form 7 August 2019; Accepted 22 August 2019
Available online 18 September 2019

contribution to the ERG is evident as a series of positive and negative deflections after flash on– and off-set that are different to the cone-directed ERG waveforms (Fukuda et al., 2012). Given this incongruity, the melanopsin contribution to the ERG is unclear.

To measure the electrical responses from rods and cones, conventional ERG techniques mainly either use stimulus flashes presented against a dark background, or apply variable states of light adaptation (McCulloch et al., 2015); these methods quantify the relative activity of the rod and cone photoreceptors using different stimulus contrast and adaptation conditions. Recently, a temporal white noise ERG (wnERG) technique was introduced to render a continuous measurement of the ERG responses under retinal equilibrium set by constant light adaptation (Zele et al., 2017). The wnERG resembles a typical flash ERG with a negative (N1) and positive (P1) waveform (Zele et al., 2017). This method can be easily combined with silent-substitution techniques to control photoreceptor-specific pathways and their interactions. The first aim of this study is to determine whether a measurable waveform can be derived from the human wnERG to melanopsin-directed stimuli under conditions that independently control the excitation of melanopsin cells without changing the excitation of rod and cone photoreceptors.

Melanopsin cells receive extrinsic light inputs from the outer retinal rods and cones via bipolar cells (Belenky, Smeraski, Provencio, Sollars, & Pickard, 2003; Dacey et al., 2005; Grünert et al., 2011; Güler et al., 2008; Jusuf, Lee, Hannibal, & Grünert, 2007; Liao et al., 2016; Nasir-Ahmad et al., 2019). In mice, melanopsin cells also form intra-retinal collaterals that may mediate a retrograde signalling from melanopsin cells via dopaminergic amacrine cells to bipolar cells as well as rods and cones (Newkirk, Hoon, Wong, & Detwiler, 2013; Zhang, Belenky, Sollars, Pickard, & McMahon, 2012; Zhang et al., 2008). The implication of melanopsin-mediated retrograde signalling pathways in the human retina is not known. A possible role for this pathway is for melanopsin to modulate outer retina signalling via feedback mechanisms. Therefore, the second aim of this study is to investigate whether melanopsin influences cone function in humans as measured using the photopic wnERG.

2. Materials and methods

2.1. Observers and ethical approval

Ten participants were recruited, including nine observers with trichromatic colour vision (3 females, 6 males, 23–41 years) and one deuteranomalous trichromat (male, 34 years). They had no systemic disease and no retinal or optic nerve disease as confirmed by a comprehensive ophthalmic examination, including fundus examination, optical coherence tomography (RS-3000 OCT RetinaScan Advance; Nidek Co. Ltd., Tokyo, Japan), colour vision (D-15 and Rayleigh colour match), visual acuity (Bailey-Lovie Log MAR Chart), contrast sensitivity (Pelli-Robson) and intra-ocular pressure (tonometer, iCare Finland Oy, Helsinki, Finland). Not all 10 observers participated in all experimental conditions (see Section 2.6). All experimental protocols were approved by the Queensland University of Technology (QUT) Human Research Ethics Committee (approval no.: 1400000543) and conducted in accordance with their guidelines. The research followed the tenets of the Declaration of Helsinki and informed consent was obtained from all participants.

2.2. Apparatus and physical calibration

A 5-primary photostimulator (Cao et al., 2015) generated a 30° outer diameter annular test field with a central 10.5° diameter macular block that was used to independently modulate the melanopsin, rod and three cone photoreceptor (L-, M-, and S-cone) excitations using the principle of silent-substitution (Estévez & Spekreijse, 1982). The photostimulator comprised five narrowband primary light-emitting diodes (LEDs) and interference filters. The peak wavelengths (and full widths at half maximum) of the LEDs and interference filter combinations were 456 nm (10 nm), 488 nm (11 nm), 540 nm (10 nm), 594 nm (14 nm), and 633 nm (15 nm). The lights from the primaries were combined using fibre optic cables and a homogeniser; the combined light was focussed by a field lens at the pupil in a Maxwellian view (Cao et al., 2015). The primary light outputs were regulated by an Arduino based stimulation system, LED driver (TLC5940), microcontroller (Arduino Uno SMDR3, Model A000073) and calibrated neutral density filters (Ealing, Natick, MA, USA) using custom designed software (Xcode 3.2.3, 64-bit, Apple, Inc., Cupertino, CA, USA). The system provided a 12-bit resolution and a high frequency limit of ~488 Hz. The spectral outputs of the five primaries were measured with an EPP2000C-50 μm Slit UV–VIS Spectrometer (StellarNet, Tampa, FL, USA).

The cone (LMS), rod (R) and melanopsin (I) excitations were calculated based on the CIE 1964 10° standard observer cone fundamentals (Smith & Pokorny, 1975), CIE 1951 scotopic luminosity function, and melanopsin spectral sensitivity function (al Enezi et al., 2011), respectively. For an equal energy spectrum light at 1 photopic Td, the photoreceptor excitation relative to photopic luminance with a 2:1 L:M cone ratio (Smith & Pokorny, 1975) is $l = L/(L + M) = 0.6667$, $m = M/(L + M) = 0.3333$, $s = S/(L + M) = 1$, $r = R/(L + M) = 1$, $i = I/(L + M) = 1$. To obtain the maximum instrument gamut for the photoreceptor-isolating conditions, an orangish adapting field was chosen ($l = 0.752$, $s = 0.105$, $r = 0.319$ and $i = 0.235$; 1931 CIE $x = 0.549$, $y = 0.410$). To calculate the electric current requirements for the primaries to produce the pre-determined photoreceptor excitation, the luminance outputs of each primary were measured at a range of 1024 current levels using an ILT1700 Research Radiometer (International Light Technologies, Inc., Peabody, MA, USA). The luminance outputs and currents were normalised to the maximum to calculate the linearisation coefficients that were used to calculate the linearised current levels (Cao et al., 2015; Zele, Fiegl et al., 2018).

2.3. Observer calibration

Individual differences in ocular media density and the occurrence of photopigment polymorphisms cause differences in the retinal illuminance and photoreceptor excitation and therefore introduce inadvertent photoreceptor intrusions in the calculation of photoreceptor-isolating conditions. To compensate for individual differences in pre-receptoral filtering and photoreceptor spectral sensitivities between the observer and the CIE 1964 10° standard observer, Heterochromatic Flicker Photometry (HFP) was completed for each observer. The HFP procedure used a Cyan primary flickering at 100 Td (Talbot illuminance of 50 Td; 15 Hz rectangular-waveform) as a reference and the observer adjusted the illuminance of a test primary (Blue, Green, Amber or Red) to minimise the appearance of flicker. The 15 Hz flicker is mediated by the luminance pathway (Guth & Lodge, 1973; Smith & Pokorny, 1975) because it is beyond the critical fusion frequency of the chromatic pathways (Brindley, Du Croz, & Rushton, 1966; Swanson, Ueno, Smith, & Pokorny, 1987) and the melanopsin pathway (Zele, Fiegl et al., 2018). The ratio of the retinal illuminance of the test primary to that of the Cyan primary was used to adjust the output of the test primary so that the relative photoreceptor excitation of the observer is consistent with the 10° standard observer.

The spectral distributions of the five primary lights (Blue, Cyan, Green, Amber and Red) measured at their maximal outputs are $P_1(\lambda)$, $P_2(\lambda)$, $P_3(\lambda)$, $P_4(\lambda)$, $P_5(\lambda)$. The photoreceptor excitation for the ith primary based on the photoreceptor spectral sensitivity for the jth photoreceptor (S, M, L cone, rod, or melanopsin) was then computed as

$$E_{i,j} = \int P_i(\lambda) f_j(\lambda) \quad (1)$$

We then created an A-matrix (A) with each row representing the photoreceptor excitations [S M L R I: S-cones, M−cones, L-cones, rods

(R) and melanopsin (I)] for the standard observer at the maximum output of the *i*th primary (Eq. (2)).

$$A = \begin{bmatrix} S_1 & M_1 & L_1 & R_1 & I_1 \\ S_2 & M_2 & L_2 & R_2 & I_2 \\ S_3 & M_3 & L_3 & R_3 & I_3 \\ S_4 & M_4 & L_4 & R_4 & I_4 \\ S_5 & M_5 & L_5 & R_5 & I_5 \end{bmatrix} \quad (2)$$

To display a light for a specific combination of five photoreceptor excitations β = [S M L R I], the unique scaling coefficient for each primary can be found as $\alpha = [p_1\ p_2\ p_3\ p_4\ p_5] = \beta A^{-1}$, where p_i represents the proportion relative to its maximum for the *i*th primary. For an individual observer, the photoreceptor excitations are $E_{i,j} = k_i \int P_i(\lambda) f_j(\lambda)$; we estimated k_i based on HFP. For example, for the Blue primary, the illuminance required to equate Cyan (C_L) is B_L, then k_B for the Blue primary will be C_L/B_L; k_C will be 1 for the reference Cyan primary. Then,

$$A' = \begin{bmatrix} k_1S_1 & k_1M_1 & k_1L_1 & k_1R_1 & k_1I_1 \\ k_2S_2 & k_2M_2 & k_2L_2 & k_2R_2 & k_2I_2 \\ k_3S_3 & k_3M_3 & k_3L_3 & k_3R_3 & k_3I_3 \\ k_4S_4 & k_4M_4 & k_4L_4 & k_4R_4 & k_4I_4 \\ k_5S_5 & k_5M_5 & k_5L_5 & k_5R_5 & k_5I_5 \end{bmatrix} \quad (3)$$

Following this, the light displayed for the individual observer will be based on *A'* instead of the A-matrix (*A*). This arrangement ensured that the excitation of a given photoreceptor class for a given stimulus contrast remained constant across all individual observers, including the one deuteranomalous trichromat.

HFP performed at ≤100 Td provides more precise estimates of luminance efficiency than that performed at higher illuminances (Pokorny, Jin, & Smith, 1993) and these estimates are applicable to up to ~2,380 cd.m^{-2} luminances (~8,000 Td) (Burns, Elsner, Lobes, & Doft, 1987); our highest adaptation level was ~1,600 cd.m^{-2} (~80,000 Td). The 80,000 Td illuminance was achieved by pupil dilation and thus increasing the retinal area stimulated. Such high photopic stimuli therefore would not alter the amount of photoreceptor bleaching and would rather increase the number of photoreceptors (retinal area) that are bleached by the same amount. This implies that our luminous efficiency estimates based on HFP at 100 Td would be applicable to these higher photopic illuminances. We have performed multiple measurements detailed elsewhere to confirm the observer calibration and photoreceptor isolation (Zele et al., 2019b; Zele, Feigl et al., 2018).

2.4. Temporal white noise electroretinogram (wnERG)

The temporal white noise (TWN) stimuli allow for a continuous recording of the ERG. Furthermore, the whole period of the ERG recording is used for cross-correlation with the noise stimulus (i.e. without re-adaptation periods as with flash ERGs; see below) so that the signals can be averaged to increase the signal-to-noise ratio (SNR) (Zele et al., 2017). We measured the wnERG to the TWN stimuli that modulate around a mean adaptation level to allow independent control of the photoreceptor contributions to the ERG when applied in conjunction with the silent-substitution technique. The TWN stimulus was presented in 1 s epochs containing 1024 photoreceptor excitations evenly distributed in the 0 to 64 Hz frequency range (Adhikari, Zele, Cao, Kremers, & Feigl, 2018) with a Gaussian distribution around the mean luminance (Fig. 1A, B, C) and the phase randomly varied between 0° to 359° and repeated 40 times, as per the methodology introduced by Zele et al. (2017). The inverse fast Fourier transform shows that in the frequency domain the white noise had equal amplitudes at all temporal frequencies between 0 and 64 Hz (Fig. 1D). To increase the SNR by decorrelating the ERG signal from the line frequency, each 1 s epoch of the temporal white noise stimulus was separated by a 1 ms blank interval (Zele, Feigl, Kambhampati, Hathibelagal, & Kremers, 2015). The noise stimulus was cross-correlated with the wnERG waveform (Fig. 1E) to derive the impulse response function (IRF) (Fig. 1F); these calculations are detailed in Zele et al. (2017). Signal processing was performed using custom written MATLAB software (R2016a; Mathworks, Natick, MA). Epochs with voltages beyond a predefined window due to blinks and large eye movements were detected and rejected using a pre-processing algorithm (Zele et al., 2015). When using circular cross-correlation, the stimulus and response are time locked to maximise the IRF amplitude (Abboud & Sadeh, 1984; Rhudy, Bucci, Vipperman, Allanach, & Abraham, 2009); it is a standard practice in multifocal ERGs to time-lock the cross-correlation to the particular response of interest (Keating, Parks, Smith, & Evans, 2002) which typically occurs between 0 and 100 ms after stimulus onset (Hood et al., 2012). Here, the cross-correlation analysis was defined by the wnERG (1 s duration) and response (1 s duration) epochs sharing the same time reference; matching the time-locked epochs ensured each time series was completely represented in the IRF.

To determine melanopsin contributions to the wnERG and their effect on cone signalling, the continuous wnERG was recorded in response to (1) melanopsin-directed TWN stimuli that did not change the rod, L-, M- or S-cone photoreceptor excitations, (2) with LMS-cone-directed TWN stimuli that did not change the rod or melanopsin photoreceptor excitations, and (3) with combined melanopsin and cone-directed TWN stimuli that did not change the rod photoreceptor excitations. The stimulus contrasts and frequency range were limited by the instrument gamut, and we used the maximum range possible. The inter-session standard error of the mean (SEM) for the implicit times of the wnERG components in one representative observer ranged from 1.2 to 3.1 ms (similar in other observers), consistent with inter-individual variability reported in wnERGs and flash ERGs (Zele et al., 2017). The SEMs are also less than the proposed threshold criterion of 4.3 ms used for detecting a significant change in the light adapted flash ERG implicit times (Grover, Fishman, Birch, Locke, & Rosner, 2003).

2.5. ERG procedure

The ERG set up was conducted according to the International Society for Clinical Electrophysiology of Vision (ISCEV) standards (McCulloch et al., 2015). The pupil of the right eye was dilated to at least 8 mm dimeter with 0.5% Tropicamide (Minims, Chauvin Pharmaceuticals Ltd., Romford, UK). An active fibre electrode was placed across the lower conjunctiva; the forehead (ground electrode) and temple (reference electrode) were scrubbed with alcohol and abrasive gel (Nuprep; D.O. Weaver & Co., Aurora, CO) before placing the Ag/AgCl cup electrodes filled with transmission gel (Aquasonic; Parker Laboratories, Inc., Fairfield, NJ). The observers adapted to the field for one minute prior to the recordings. The continuous wnERG was recorded from the right eye. The ERG settings and recording procedures are detailed elsewhere (Zele et al., 2017, 2015).

2.6. wnERG experiments

To measure the wnERG to melanopsin-directed stimuli and to determine the influence of melanopsin activation on cone signalling, we conducted four experiments and measured the wnERG for three photoreceptor-isolating conditions: (1) melanopsin-directed temporal white noise with no change in the rod and L-, M- and S-cone photoreceptor excitations, (2) LMS-cone-directed noise with no change in the rod and melanopsin excitation, and (3) additive LMS + melanopsin noise. As a control condition, the ERG was measured in a selected observer to the steady adaptation field with constant SMLRi photoreceptor excitations and no TWN stimulus.

Experiment 1 (n = 10 observers) determined the wnERG response to melanopsin-directed temporal white noise stimuli (36% Michelson Contrast; 0 to 64 Hz frequency range) at a mean adaptation level of 80,000 Td (1,592 cd.m^{-2}, 3.2 log cd.m^{-2}) (see section 3.1 for Results).

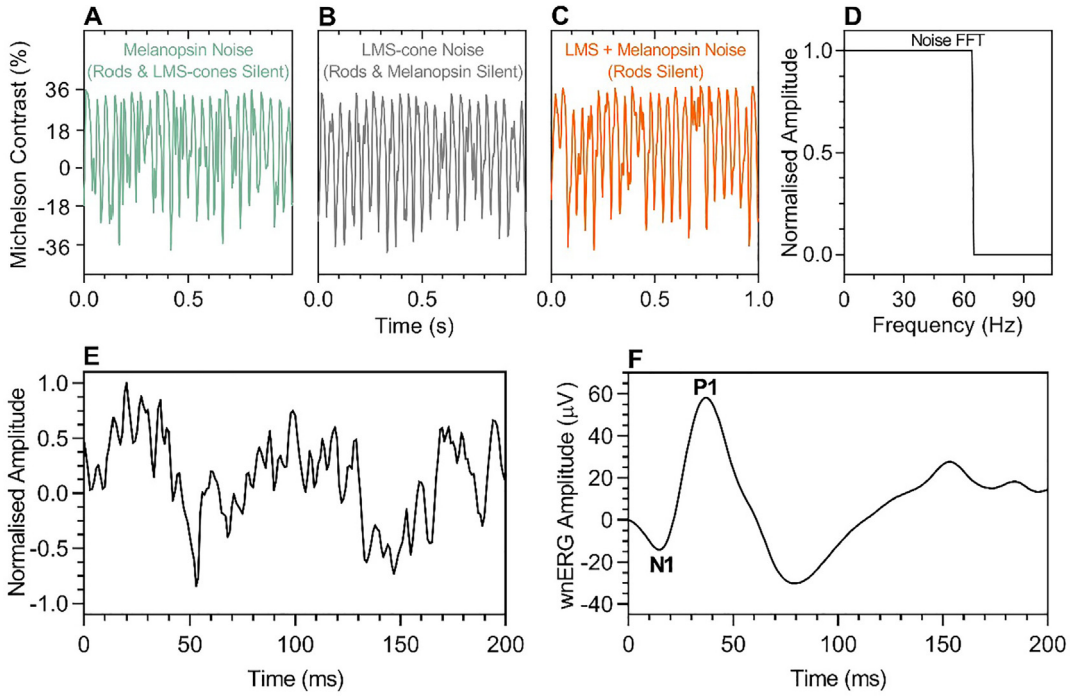

Fig. 1. Photoreceptor-isolating temporal white noise conditions used to generate the wnERG. (A) Melanopsin-directed stimuli, (B) LMS-cone-directed stimuli, (C) additive LMS + melanopsin stimuli. (D) The inverse fast Fourier transform of every condition shows constant amplitudes across the given frequency range (0 to 64 Hz). (E) Exemplar raw human wnERG waveform recorded in response to LMS-cone-directed temporal white noise (36% Michelson contrast; 0–64 Hz frequency range) and (F) the derived impulse response function (IRF) with the wnERG components, N1 and P1 indicated.

We hypothesised that the wnERG to a melanopsin-directed stimulus measured under steady-state, light-adapted conditions will reflect the combined response of the intra-retinal melanopsin pathways with waveform components having a temporal signature different to that observed in response to cone-directed stimuli. The wnERG to LMS-cone-directed stimuli (36%, 0 to 64 Hz) were also recorded for comparison.

Experiment 2 (n = 4 observers) explored whether the wnERG to melanopsin-directed stimuli could be explained by open-field and/or penumbral cone photoreceptor intrusions because of incomplete photoreceptor isolation. To simulate cone intrusion, the contrast of the LMS temporal white noise was varied (2%, 13%, 25%, 36%) and added to the melanopsin-directed stimulus (21%). The lowest LMS contrast was set to 2% because for the melanopsin-directed stimulus, the open-field LMS-cone contrast was 1.3% and the penumbral LMS-cone contrast was 1.4%. The open-field cone intrusion in melanopsin-directed stimuli was calculated as the difference between the theoretical and measured SMLRi excitations. The penumbral cone intrusion due to light absorption by the retinal vasculature was determined by calculating the spectral irradiance of each primary received by penumbral cones using haemoglobin absorption (see Zele, Feigl et al., 2018 for details). We hypothesised that cone intrusion would become evident in the wnERG at higher contrast levels (> 2%) as N1 and P1 waves with similar timing to that observed with the cone-mediated wnERG (Zele et al., 2017) and that amplitudes increase with higher LMS noise contrasts. In other words, the absence of N1 and P1 waves in the wnERG to melanopsin-directed stimuli (Experiment 1) rules out cone intrusion.

Experiment 3 (n = 4 observers) determined the intensity response and contrast response of the melanopsin-directed wnERG. The intensity response was measured at four photopic retinal illuminances (32,000, 43,000, 58,000 and 80,000 Td) at a fixed contrast (36%) and the contrast response at four melanopsin noise contrasts (10%, 19%, 28% and 36%) at a fixed retinal illuminance (80,000 Td). Given that melanopsin cellular response increases with increasing irradiance (Berson et al., 2002; Dacey et al., 2005), we hypothesised that the amplitude of the melanopsin-directed wnERG would increase with illuminance and melanopsin contrast.

Experiment 4A (n = 10 observers) explored the influence of melanopsin activation on the LMS-cone-directed wnERG by measuring the wnERG to additive LMS (36%, 0 to 64 Hz) + melanopsin (21%, 0 to 15 Hz) stimuli at 80,000 Td mean adaptation level and comparing it to the wnERG to LMS-cone-directed stimuli (36%, 0 to 64 Hz) measured in Experiment 1. Given melanopsin activation can suppress the b-wave amplitude of the cone-mediated flash ERG in mice (Allen & Lucas, 2016), we hypothesised that melanopsin activation will suppress the LMS-cone-mediated human wnERG. Our continuous wnERG allows us to evaluate if the suppression can be predicted by destructive interference between signals arising in the cone and melanopsin pathways.

Experiment 4B (n = 4 observers) determined the effect of retinal illuminance and melanopsin contrast on the LMS + melanopsin-directed wnERG. We measured the intensity response to the LMS-cone-directed stimuli (36%) and the additive LMS (36%) + melanopsin (21%) stimuli at four photopic retinal illuminances (32,000, 43,000, 58,000 and 80,000 Td) as well as the contrast response to the LMS + melanopsin stimuli with a fixed LMS contrast (36%) and variable melanopsin contrast (0%, 10%, 14%, 18% and 21%). 'Intensity response' is the term used in the ERG literature however, we use illuminance to define the mean adaptation level and therefore hereafter use 'illuminance response' to describe the wnERG as a function of adaptation level. The deuteranomalous trichromat observer showed the same trend as the trichromats for all wnERG metrics and therefore was included in the analyses.

2.7. Statistics

The data frequency distributions were evaluated with the D'Agostino and Pearson omnibus normality test. The wnERG metrics for melanopsin-directed wnERGs vs. LMS-cone wnERGs and the wnERG metrics for LMS-cone wnERGs vs. LMS + melanopsin wnERGs were compared with a paired *t*-test (normal data) or the Wilcoxon test (non-normal data) (95% confidence interval, $p < 0.05$). The illuminance

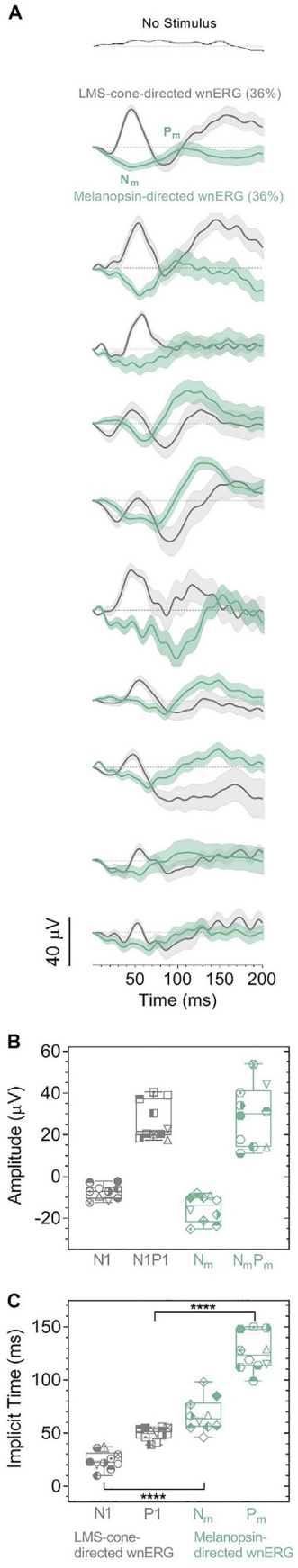

Fig. 2. Melanopsin- and cone-directed wnERGs. (A) The wnERG IRFs for each observer in response to melanopsin-directed stimuli (green lines; mean ± SEM) and LMS-cone-directed stimuli (grey lines); the black trace in the top IRF shows the response for one observer to a steady adaptation field without a temporal white noise stimulus. (B) The amplitudes and (C) implicit times of the wnERG components; the N_m and P_m waves for melanopsin-directed stimuli and the N1 and P1 waves for LMS-cone-directed stimuli are shown using a unique symbol for each observer. Asterisks indicate significance (****$p < 0.0001$; see text for details). n = 10 observers; mean retinal illuminance = 80,000 Td.

and contrast responses were analysed with linear regression. All statistical analyses were conducted with GraphPad Prism (GraphPad Software, Inc., CA, USA).

3. Results

3.1. Experiment 1: Melanopsin contributions to the wnERG

In all 10 observers, the IRF of the wnERG to the LMS-cone directed stimuli (Fig. 2A, grey lines) resembled a typical photopic flash electroretinogram (Zele et al., 2017), with a negative (N1) then a positive (P1) deflection. A blank steady adaptation field (i.e. no temporal white noise) did not elicit a wnERG IRF (Fig. 2A, black line, top panel). In all 10 observers, the IRF of the wnERG measured with melanopsin-directed stimuli (Fig. 2A, green lines) had a negative deflection (which we labelled N_m) on average at 62.9 ± 3.3 ms (mean ± SEM) followed by a positive deflection (which we labelled P_m) at 126.3 ± 5.1 ms. Fig. 2B,C show the distribution of the individual amplitudes and implicit times of N_m and P_m compared to the LMS-cone wnERG N1 and P1. The N_m implicit times of the wnERG to melanopsin-directed stimuli (62.9 ± 3.3 ms; Fig. 2C) were significantly slower ($t_9 = 8.6$, $p < 0.0001$) than the N1 implicit times of the LMS-cone directed wnERGs (24.1 ± 2.4 ms); the P_m implicit times (126.3 ± 5.1 ms; Fig. 2C) were also significantly slower ($t_9 = 13.0$, $p < 0.0001$) than the P1 implicit times (49.7 ± 1.8 ms; Fig. 2C).

3.2. Experiment 2: Effect of cone intrusion on the melanopsin-directed wnERG

In addition to the psychophysical methods used to confirm the individual observer calibrations (Sections 2.3 and 2.4), we evaluated the accuracy of the photoreceptor isolation by simulating the effect of cone intrusion on the melanopsin-directed wnERG. In a subset of four observers, the cone intrusion was simulated by combining a fixed contrast melanopsin-directed stimulus (21% Michelson contrast) with a variable contrast LMS-cone-directed stimulus (2% to 36% Michelson contrast); the N1 and P1 components of the wnERG were analysed.

Fig. 3A shows in one representative observer that at the 2% contrast level, which is above the upper range of the expected potential open-field or penumbral cone intrusion, there were no measurable N1 or P1 waves with the combined melanopsin and LMS-cone stimulus. It signifies that the wnERG response to the melanopsin-directed stimuli in Fig. 2 is not explained by cone intrusion resulting from inaccuracies in the photoreceptor isolation. At the next highest level that was measured (13% cone contrast), the N1 and P1 waves were present and then increased in amplitude with increasing LMS-cone contrast as expected in cone wnERGs (Zele et al., 2017). The group data in Fig. 3B show that the N1 amplitudes ($r^2 = 0.33$, $F_{1,14} = 6.7$, $p = 0.02$; μV = -0.1*Contrast + 0.6) and N1P1 amplitudes ($r^2 = 0.70$, $F_{1,14} = 32.4$, $p < 0.0001$; μV = 0.4*Contrast + 0.7) increased with increasing cone contrast (Fig. 3B). The implicit times were independent of cone contrast (Fig. 3C).

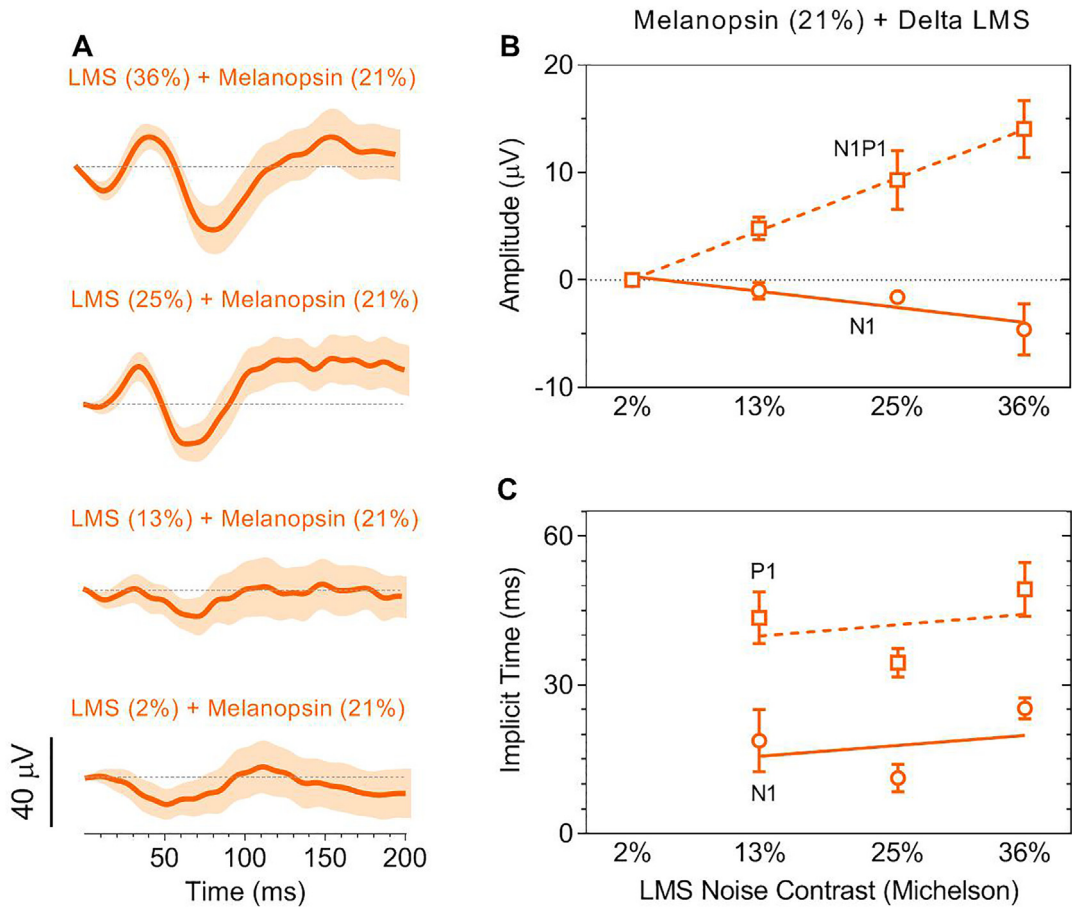

Fig. 3. Effect of cone intrusion on the melanopsin-directed wnERG. (A) The wnERG IRFs (mean ± SEM) of one representative observer in response to melanopsin-directed stimuli with different levels of LMS-cone contrast. (B) Mean (± SEM) amplitudes and (C) implicit times of the wnERG components (n = 4 observers), N1 wave (circles) and P1 wave (squares) for melanopsin-directed stimuli (21% Michelson contrast) with simulated cone intrusions (Delta LMS). There were no measurable N1 or P1 at 2% LMS-cone contrast and therefore there are no corresponding implicit times in panel C. The lines show the best-fitting linear regressions. Mean retinal illuminance = 80,000 Td.

3.3. Experiment 3: Illuminance and contrast response of the melanopsin-directed wnERG

After ruling out cone intrusion as the reason for the N_m and P_m in the wnERG to the melanopsin-directed stimulus (Experiment 2), we determined the illuminance response (n = 4 observers) and contrast response (n = 9) of the N_m and P_m in Experiment 3. Fig. 4 shows the N_m amplitudes (Fig. 4A; $r^2 = 0.63$, $F_{1,14} = 23.7$, $p = 0.0002$; µV = -41.2*Td + 182.4) and N_mP_m amplitudes (Fig. 4A; $r^2 = 0.41$, $F_{1,14} = 7.6$, $p = 0.02$; µV = 58.5*Td − 243.9) increased with increasing field retinal illuminance. The N_m amplitudes (Fig. 4B; $r^2 = 0.35$, $F_{1,34} = 18.1$, $p = 0.0002$; µV = -0.4*Contrast − 1.1) and N_mP_m amplitudes (Fig. 4B; $r^2 = 0.33$, $F_{1,34} = 16.9$, $p = 0.0002$; µV = 0.9*Contrast − 3.8) also increased with increasing melanopsin noise contrast. The N_m and P_m implicit times were independent of the field retinal illuminance (Fig. 4C) as well as melanopsin noise contrast (Fig. 4D).

3.4. Experiment 4A: Effect of melanopsin activation on the cone-directed wnERG

To determine the influence of melanopsin activation on the LMS-cone-directed wnERG, Experiment 4A (n = 10 observers) measured the wnERG to additive LMS (36%) + melanopsin (21%) stimuli at an 80,000 Td mean adaptation level (Fig. 5). Compared to the LMS-cone-directed wnERG (36%) from Experiment 1 presented in Fig. 2 (grey lines and symbols), the additive LMS + melanopsin-directed wnERG (Fig. 5A, orange lines) had significantly lower N1P1 amplitudes ($t_9 = 8.4$, $p < 0.0001$) with no difference in the N1 amplitudes or in the timing of the N1 and P1 components (compare grey data in Fig. 2B, C vs orange data in Fig. 5B, C). The combined melanopsin- and cone-directed noise decreased the cone N1P1 amplitude compared to the LMS-cone-directed wnERG by 58.6% on average. Given the N_m component of melanopsin-directed wnERG and the P1 component of cone-directed wnERG have opposite polarity but similar implicit times (49.7 ms vs 62.9 ms), we explored whether destructive interference between the two IRFs could predict the lower N1P1 amplitudes observed with the additive LMS + melanopsin stimuli. This simple analysis of destructive interference was conducted based on evidence that melanopsin can interact with conventional cone pathways in isolated mouse retinae in the absence of top-down regulation (Milosavljevic et al., 2018; Schmidt et al., 2014). The LMS-cone-directed and melanopsin-directed wnERG IRFs (grey and green lines from Fig. 2A) were added to derive the composite IRF traces (Fig. 5A, blue lines). The composite IRFs were similar to the IRFs with additive LMS + melanopsin stimuli with some variability; the amplitudes (Fig. 5B) and implicit times (Fig. 5C) were not significantly different between the two IRFs (N1 implicit times: $t_8 = 0.27$, $p = 0.80$; N1 amplitudes: $p = 0.49$; P1 implicit times: $t_8 = 0.38$, $p = 0.71$; N1P1 amplitudes: $t_9 = 1.07$, $p = 0.31$).

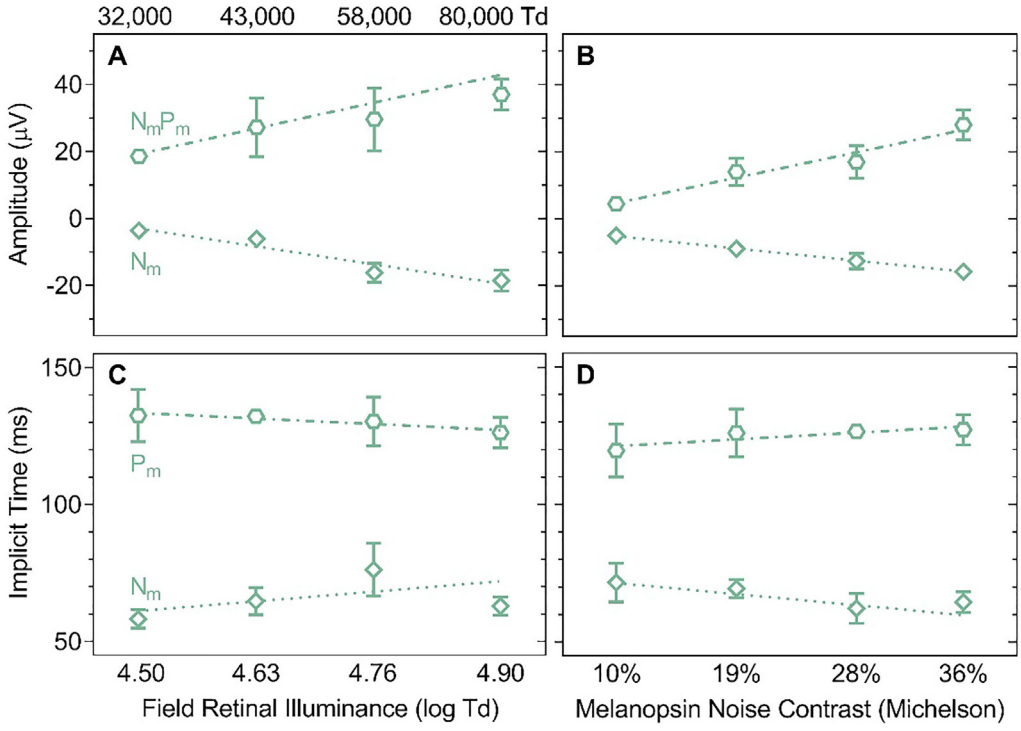

Fig. 4. Illuminance and contrast response of the melanopsin-directed wnERG. (A, B) Mean (± SEM) amplitudes and (C, D) implicit times of the N_m wave (diamonds) and P_m wave (hexagons) of the wnERGs to melanopsin-directed stimuli as a function of retinal illuminance (n = 4 observers, 36% Michelson contrast) and melanopsin noise contrast (n = 9 observers; mean retinal illuminance = 80,000 Td). The lines show the best-fitting linear regressions.

3.5. Experiment 4B: Illuminance and contrast response of the additive LMS + melanopsin wnERG

To determine the effect of retinal illuminance and melanopsin noise contrast on the additive LMS + melanopsin wnERG N1P1 amplitudes, Experiment 4B (n = 4 observers) quantified (1) the illuminance response (32,000 – 80,000 Td) to LMS-cone-directed stimuli and the additive combination of the LMS-cone and melanopsin-directed stimuli and (2) the contrast response to the additive LMS + melanopsin stimuli with a fixed LMS-cone contrast (36% Michelson contrast) and variable melanopsin contrast (0 – 21% Michelson contrast) at 80,000 Td. Fig. 6A shows that the N1 amplitudes (r^2 = 0.32, $F_{1,14}$ = 6.6, p = 0.02; μV = –15.4*Td + 67.9) and N1P1 amplitudes (r^2 = 0.65, $F_{1,14}$ = 25.7, p = 0.0002; μV = 65.7*Td − 292.1) of the LMS-cone wnERGs increased with increasing field illuminance. Fig. 6B shows that the N1 amplitudes (r^2 = 0.28, $F_{1,14}$ = 5.5, p = 0.03; μV = -11.0*Td + 48.6) and N1P1 amplitudes (r^2 = 0.41, $F_{1,14}$ = 9.5, p = 0.008; μV = 30.1*Td − 131.1) of the LMS + melanopsin wnERGs also increased with increasing field illuminance but with shallower slopes than those for the LMS wnERGs, in agreement with the results of Experiment 4A. All implicit times were independent of illuminance and the presence of additional melanopsin stimulation. The illuminance versus N1P1 response relationship was fitted with a Naka-Rushton function (Naka & Rushton, 1966) (Fig. 7A). The Naka-Rushton function for the LMS wnERGs and LMS + melanopsin wnERGs differed in the maximum response amplitude (23.0 vs. 13.5 μV) whereas the slopes (8.2 vs. 10.1) and the illuminance required to produce the half-maximum response (4.60 vs 4.58 log Td) were stable between the two conditions. The N1P1 amplitudes of the LMS wnERGs decreased with increasing the contrast of added melanopsin-directed noise (Fig. 6C; r^2 = 0.50, $F_{1,18}$ = 17.7, p = 0.0005; μV = –0.8*Contrast + 28.5). The suppression of the LMS-cone wnERG N1P1 amplitudes with the addition of melanopsin-directed noise increased with increasing field illuminance (Fig. 7B; r^2 = 0.57, $F_{1,14}$ = 18.7, p = 0.0007; μV = 35.7*Td − 161.0).

4. Discussion

We present evidence that the melanopsin-directed wnERG gives rise to a waveform with negative (N_m) and positive (P_m) deflections (Fig. 2) that are ~39 ms and 77 ms slower than the cone wnERG N1 and P1 waves, respectively. Control experiments demonstrate this waveform is not generated by cone intrusion (Fig. 3). Instead, this waveform may represent the combined activity of the intrinsic melanopsin response and the post-melanopsin pathways because the wnERG was measured under conditions in which the retina was in a state of equilibrium set by the steady adaptation level during the continuous ERG recording. This contrasts with a flash ERG in response to a single stimulus recorded during a single epoch that is dominated by sequential outer retinal contributions.

Given that the success of the silent substitution methodology is reliant on the accuracy of the photoreceptor isolating conditions, we conducted a series of tests to establish this (Fig. 3 and Section 2.3). We also highlight that other studies have demonstrated that melanopsin- and cone- directed stimuli produce different pupil responses, indicative of the different photoreceptor and afferent pathways mediating their response (Barrionuevo & Cao, 2016; Barrionuevo, McAnany, Zele, & Cao, 2018; Barrionuevo et al., 2014; Zele et al., 2019a; Zele, Feigl et al., 2018). Theoretically, our stimuli were silent for rods (i.e. produce no change in the rod photoreceptor excitation); for our high photopic light levels (≥32,000 Td – 80,000 Td) the observers were also light-adapted to the field for at least one minute prior to each recording. Cone-mediated wnERGs show typical N1 and P1 waves (Zele et al., 2017), and when cone stimulation is added to the melanopsin-directed stimuli, the amplitudes of these waves are cone contrast dependent (Fig. 3), but have no intrusion at contrast levels that might be expected to arise from open-field and/or penumbral cones due to incomplete photoreceptor isolation. The characteristic wnERG to melanopsin-directed stimuli also had a waveform shape different to that observed in a typical cone ERG. Taken together, the slow negative and positive deflections observed in the wnERG to the melanopsin-directed stimuli are not likely to be due to cone or rod intrusion.

We infer that the melanopsin-directed wnERG represents the combined response of intrinsic melanopsin activity as well as the intra-retinal feedback to amacrine cells and potentially to Müller cells and the RPE. Melanopsin cells have intra-retinal connections to dopaminergic amacrine cells for retrograde feedback pathways (Newkirk et al.,

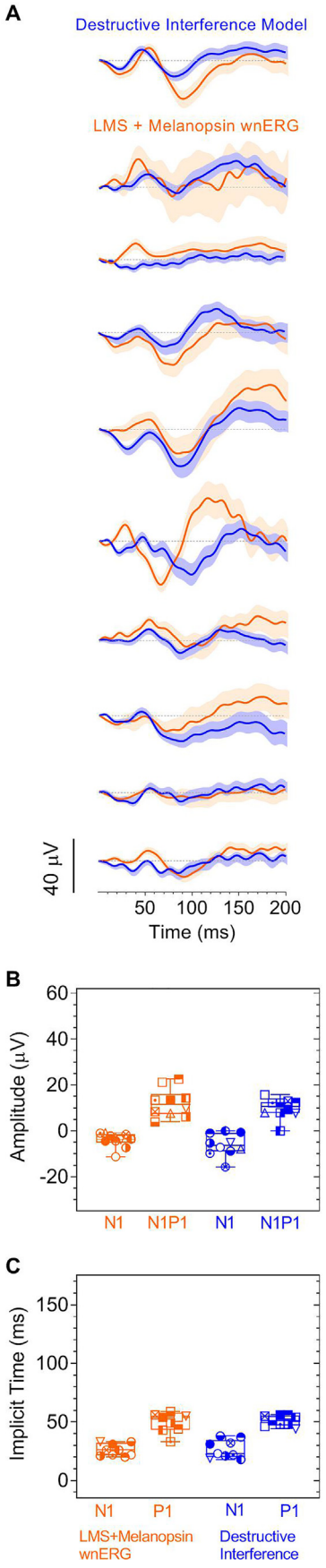

Fig. 5. Combined melanopsin- and cone-directed wnERGs. (A) The composite wnERG IRFs (blue lines; mean ± SEM) were generated by mathematically adding the measured LMS-cone-directed wnERG and melanopsin-directed wnERG IRFs (both from Fig. 2A); these composite wnERGs (blue lines) are overlaid with the wnERG IRFs measured for each observer in response to the additive LMS + melanopsin stimuli (orange lines) (n = 10 observers). (B) Amplitudes and (C) implicit times of the wnERG components; N1 and P1 waves are shown for each observer indicated by a unique symbol. Mean retinal illuminance = 80,000 Td. (For interpretation of the references to colour in this figure legend, the reader is referred to the web version of this article.)

2013; Zhang et al., 2012; Zhang et al., 2008) and there is evidence that melanopsin cells rely on connections to Müller cells and the retinal pigment epithelium for photopigment regeneration at high irradiances (Zhao, Pack, Khan, & Wong, 2016). The melanopsin-directed wnERG to continuous recordings under steady adaptation level may therefore reflect an indirect consequence of the activity of the melanopsin pathway. It does not however, reveal the melanopsin depolarisation to light onset (Berson et al., 2002; Dacey et al., 2005) unlike a single flash ERG that represents the direct hyperpolarisation of outer retinal photoreceptors and depolarisation of bipolar cells (Brown, 1968). A direct comparison is therefore not possible between the implicit times of the melanopsin-directed wnERG measured under high photopic adaptation levels and in vivo electrophysiological recordings of melanopsin depolarisation measured in dark-adapted retinae. As melanopsin cells also provide retrograde signals to cones and bipolar cells (Zhang et al., 2008), we cannot exclude the possibility that the slow melanopsin-directed wnERG components include responses arising from the cone pathway after receiving melanopsin feedback. Further studies under pharmacological blockage of individual cellular contributions in the anterograde and retrograde melanopsin pathways in animal models are required to ascertain the origin of the waveform components of the melanopsin-directed wnERG.

There have been previous evaluations of the melanopsin contribution to the light-adapted flash ERG in mice (Allen & Lucas, 2016) and humans (Fukuda et al., 2012). The flash ERG to a melanopsin-directed incremental pulse (50 ms, 87% Michelson contrast with ~ 900 Td, full-field adaptation) recorded during a 700 ms epoch was not measurable (Allen & Lucas, 2016). Increasing the incremental pulse duration is known to reveal on– and off-signal components (Alpern & Faris, 1956; Johnson & Bartlett, 1956) in the ERG that reflect activity of the ON– and OFF-pathways (Brown, 1968). With longer duration, 250 ms melanopsin-directed incremental pulses (50% Michelson contrast) measured at a higher adaptation level (~27,000 Td, 28.1° diameter focal stimulation) and recorded during a 1000 ms epoch, Fukuda et al. (2012) showed evidence for a melanopsin contribution to the flash ERG as a series of positive and negative deflections present after flash onset and offset. The wnERG paradigm (Zele et al., 2017) is however different to the flash ERG paradigm because it maintains both a constant adaptation level (i.e. steady light adaptation) and photoreceptor excitation such that the retina is in a state of equilibrium during the entire, continuous recording. We therefore anticipate the melanopsin-directed wnERG waveform is different to that measured with incremental pulses (flash ERG). Similar to Fukuda et al. (2012) however, we observered melanopsin-driven wnERGs at high illuminances, and our pilot experiments showed they were not measurable below 32,000 Td. That our illumination levels were higher than Fukuda et al. (2012) is due to our application of a smaller stimulus area incorporating a central 10.5° macular blocker with the 30° outer diameter stimulus. There is a lower level of photopigment expression on ipRGCs per unit area compared to rods and cones (Do et al., 2009) and we expect that larger, focal stimuli, or full-field illumination would produce larger signal amplitudes, and that perhaps these signals would then be observable at lower retinal illuminances.

There is evidence from mouse models that the melanopsin pathway can modulate the b-wave amplitude of the cone ERG; the diurnal

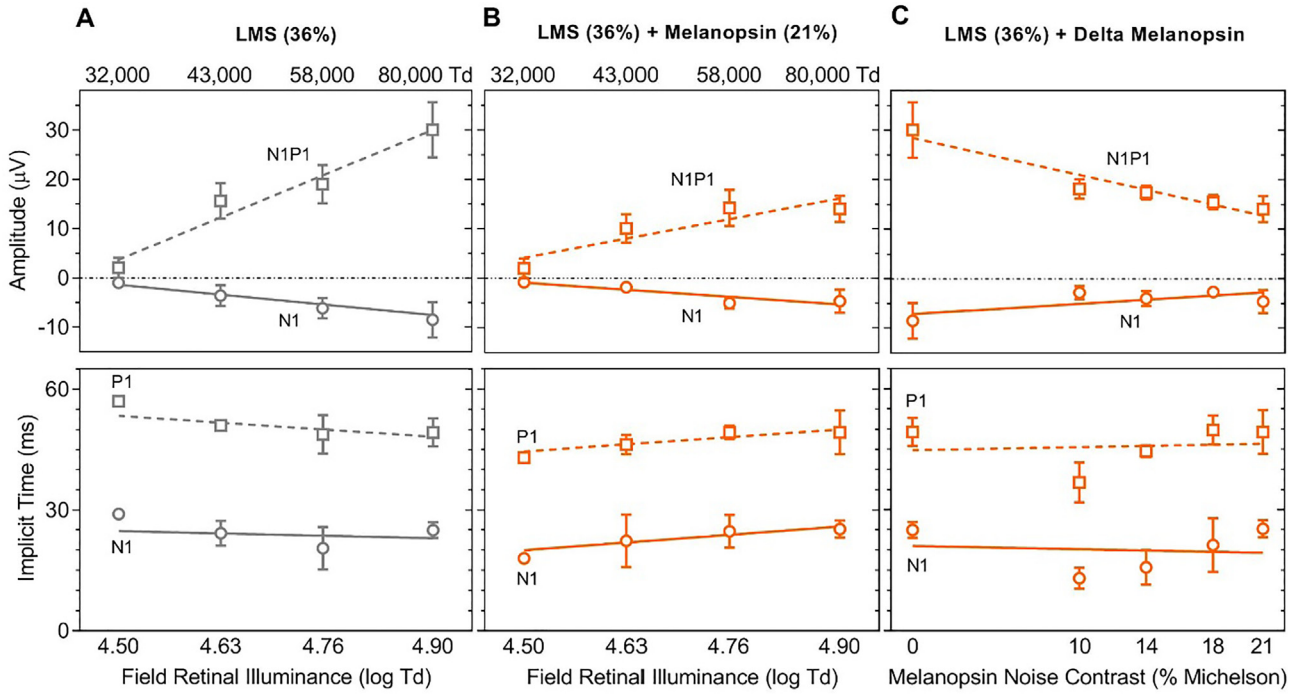

Fig. 6. Illuminance and contrast response of the additive LMS + melanopsin wnERG. Mean (± SEM) amplitudes (upper panels) and implicit times (lower panels) of the N1 wave (circles) and P1 wave (squares) for (A) LMS-cone wnERGs at variable illuminances, (B) additive LMS + melanopsin wnERGs at variable illuminances, and (C) additive LMS + melanopsin wnERGs with variable melanopsin contrast (mean retinal illuminance = 80,000 Td). The lines show the best-fitting linear regressions (n = 4 observers).

variation of the b-wave amplitude observed in wild-type mice is attenuated in melanopsin knock-out mice (Barnard, Hattar, Hankins, & Lucas, 2006) and genetic ablation of M1 ipRGCs eliminates the time-dependent (6 min) increase in the light-adapted b-wave amplitude seen in the wild-type (Prigge et al., 2016). We show that the combined melanopsin- and cone-directed noise decreases the N1P1 amplitude compared to the cone-directed wnERG (Fig. 5A, B), consistent with the observed suppression of the cone flash ERG b-wave amplitude in mice with additional melanopsin stimulation (Allen & Lucas, 2016; Allen et al., 2014; Milosavljevic, Cehajic-Kapetanovic, Procyk, & Lucas, 2016). These differences in ipRGC-modulated cone signalling between mice with genetic ablation of ipRGCs and mice/humans with intact retinae indicate that genetic ablation of ipRGCs may affect cone signalling differently compared to changing melanopsin activation in intact retinae. This may be because ipRGC collaterals provide conduits for cone signals to drive dopaminergic amacrine cells (DACs) that mediate b-wave light adaptation through dopamine release (Newkirk et al., 2013). Future physiological studies might therefore consider measuring the ERG in melanopsin photopigment knockout models with intact ipRGC collaterals. The b-wave (P1 wave) arises from bipolar cells (Sieving, Murayama, & Naarendorp, 1994) and the increase or decrease of its amplitude with increasing melanopsin activation is potentially mediated by retrograde signalling from ipRGCs to bipolar cells through intra-retinal melanopsin cell collaterals to DAC dendrites (Newkirk et al., 2013; Zhang et al., 2012; Zhang et al., 2008). ipRGCs provide retrograde excitatory inputs to DACs (Newkirk et al., 2013; Zhang et al.,

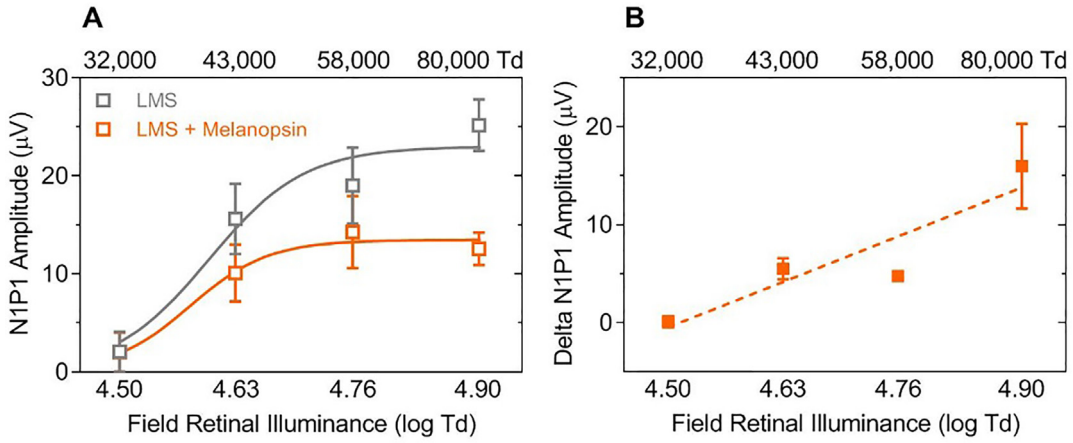

Fig. 7. Reduction in cone-directed wnERG amplitude with melanopsin stimulation. (A) The Naka-Rushton function fitted to the mean (± SEM) N1P1 amplitudes for the LMS wnERGs (grey symbols and line) and LMS + melanopsin wnERGs (orange symbols and line). (B) The magnitude of reduction in the N1P1 amplitudes of the LMS-cone wnERGs with additive melanopsin-directed noise plotted as a function of illuminance. The lines show the best-fitting linear regressions (n = 4 observers). (For interpretation of the references to colour in this figure legend, the reader is referred to the web version of this article.)

2008) whereas DACs provide anterograde inhibitory inputs to ipRGCs (Belenky et al., 2003; Viney et al., 2007; Vugler, Redgrave, Lawrence, Greenwood, & Coffey, 2007; Wong, Dunn, Graham, & Berson, 2007). Therefore, the relative weighting of these excitatory and inhibitory inputs determines whether melanopsin stimulation suppresses or increases the activity of the cone pathway, which we propose is dependent on adaptation level. At higher photopic light levels above ~15.4 log quanta.cm^{-2}.s^{-1}, the inhibitory inputs are dominant and suppress cone signalling as we observed (Fig. 5), whereas at lower photopic light levels below ~13.7 log quanta.cm^{-2}.s^{-1}, the excitatory inputs are dominant and enhance cone signalling as observed by Prigge et al. (2016). As such, melanopsin activation enhances the contrast sensitivity of conventional retinal ganglion cells and M4 ipRGCs at 9.0 to 14.0 log quanta.cm^{-2}.s^{-1} irradiances in mice (Schmidt et al., 2014; Sonoda, Lee, Birnbaumer, & Schmidt, 2018) as well as cone-mediated vision at ~14.7 log quanta.cm^{-2}.s^{-1} irradiances in humans (Zele et al., 2019b). Taken together, melanopsin expressing ipRGCs might optimise visual contrast sensitivity by modulating the gain of the cone pathway, with the modulation dependent on light level.

We show that the lower wnERG amplitudes with the combined LMS + melanopsin stimuli than with LMS-cone-directed stimuli could be reasonably well described by a destructive interference between the positive component (P1) of LMS-cone-directed IRFs and the negative component (N_m) of melanopsin-directed IRFs (Fig. 5). This destructive interference analysis assumes that melanopsin and cone signals add linearly in the retina. Whether melanopsin and cone signals combine linearly or non-linearly in the retina could depend on the relative magnitude of the retrograde excitatory inputs from ipRGCs to dopaminergic amacrine cells (DACs) and the anterograde inhibitory inputs from DACs to ipRGCs, and the magnitude may be dependent on adaptation level; further physiological studies are required to understand the anterograde and retrograde networking between ipRGCs and DACs and their implication for vision and the electroretinogram. An alternate explanation for the lower wnERG amplitudes with combined LMS + melanopsin stimuli could be that the separate cone and melanopsin wnERG signals sum at the electrode to produce a composite response, as do a number of separate components arising from different retinal cells sum to produce a typical conventional ERG waveform (Brown, 1968).

In conclusion, we recorded a characteristic wnERG waveform to melanopsin-directed stimuli that included negative and positive deflections with a waveform shape distinctly different to that generated by cone-directed stimuli. This melanopsin-directed wnERG may reflect the equilibrium response of the intra-retinal melanopsin pathway including intrinsic melanopsin photoreception as well as the activity of post-melanopsin dopaminergic amacrine cells, Müller cells and the RPE. These findings provide a new approach for objectively quantifying melanopsin signalling in humans, and can be applied in animal models.

Acknowledgements

Supported by Australian Research Council Discovery Projects ARC-DP170100274 (AJZ, BF, DC, JK), Australian Research Council Future Fellowship ARC-FT180100458 (AJZ), and a QUT Institute of Health and Biomedical Innovation Early Career Researcher Development Award (PA).

References

Abboud, S., & Sadeh, D. (1984). The use of cross-correlation function for the alignment of ECG waveforms and rejection of extrasystoles. *Computers and Biomedical Research, 17*(3), 258–266.

Adhikari, P., Zele, A. J., Cao, D., Kremers, J., & Feigl, B. (2018). The influence of melanopsin activation on the cone-mediated photopic white noise electroretinogram (wnERG) in humans. *Frontiers in Optics* (pp. JTu3A). Optical Society of America. https://doi.org/10.1364/FIO.2018.JTu3A.109.

Adhikari, P., Zele, A. J., & Feigl, B. (2015). The post-illumination pupil response (PIPR). *Investigative Ophthalmology & Visual Science, 56*(6), 3838–3849.

al Enezi, J., Revell, V., Brown, T., Wynne, J., Schlangen, L., & Lucas, R. (2011). A "melanopic" spectral efficiency function predicts the sensitivity of melanopsin photoreceptors to polychromatic lights. *Journal of Biological Rhythms, 26*(4), 314–323.

Allen, A. E., & Lucas, R. J. (2016). Using silent substitution to track the mesopic transition from rod-to cone-based vision in mice. *Investigative Ophthalmology & Visual Science, 57*(1), 276–287.

Allen, A. E., Storchi, R., Martial, F. P., Petersen, R. S., Montemurro, M. A., Brown, T. M., & Lucas, R. J. (2014). Melanopsin-driven light adaptation in mouse vision. *Current Biology, 24*(21), 2481–2490.

Alpern, M., & Faris, J. J. (1956). Luminance-duration relationship in the electric response of the human retina. *Journal of the Optical Society of America, 46*(10), 845–850.

Barnard, A. R., Hattar, S., Hankins, M. W., & Lucas, R. J. (2006). Melanopsin regulates visual processing in the mouse retina. *Current Biology, 16*(4), 389–395.

Barrionuevo, P. A., & Cao, D. (2016). Luminance and chromatic signals interact differently with melanopsin activation to control the pupil light response. *Journal of Vision, 16*(11) 29 29.

Barrionuevo, P. A., McAnany, J. J., Zele, A. J., & Cao, D. (2018). Nonlinearities in the rod and cone photoreceptor inputs to the afferent pupil light response. *Frontiers in Neurology, 9*, 1140.

Barrionuevo, P. A., Nicandro, N., McAnany, J. J., Zele, A. J., Gamlin, P., & Cao, D. (2014). Assessing rod, cone, and melanopsin contributions to human pupil flicker responses. *Investigative Ophthalmology & Visual Science, 55*(2), 719–727.

Belenky, M. A., Smeraski, C. A., Provencio, I., Sollars, P. J., & Pickard, G. E. (2003). Melanopsin retinal ganglion cells receive bipolar and amacrine cell synapses. *Journal of Comparative Neurology, 460*(3), 380–393.

Berson, D. M., Dunn, F. A., & Takao, M. (2002). Phototransduction by retinal ganglion cells that set the circadian clock. *Science, 295*(5557), 1070–1073.

Brindley, G., Du Croz, J., & Rushton, W. (1966). The flicker fusion frequency of the blue-sensitive mechanism of colour vision. *The Journal of Physiology, 183*(2), 497–500.

Brown, K. T. (1968). The electroretinogram: Its components and their origins. *Vision Research, 8*(6) 633-IN636.

Burns, S. A., Elsner, A., Lobes, L., & Doft, B. (1987). A psychophysical technique for measuring cone photopigment bleaching. *Investigative Ophthalmology & Visual Science, 28*(4), 711–717.

Cao, D., Chang, A., & Gai, S. (2018). Evidence for an impact of melanopsin activation on unique white perception. *Journal of the Optical Society of America A, 35*(4), B287–B291.

Cao, D., Nicandro, N., & Barrionuevo, P. A. (2015). A five-primary photostimulator suitable for studying intrinsically photosensitive retinal ganglion cell functions in humans. *Journal of Vision, 15*(1) 27 27.

Dacey, D. M., Liao, H.-W., Peterson, B. B., Robinson, F. R., Smith, V. C., Pokorny, J., ... Gamlin, P. D. (2005). Melanopsin-expressing ganglion cells in primate retina signal colour and irradiance and project to the LGN. *Nature, 433*(7027), 749–754.

Do, M. T. H., Kang, S. H., Xue, T., Zhong, H., Liao, H.-W., Bergles, D. E., & Yau, K.-W. (2009). Photon capture and signalling by melanopsin retinal ganglion cells. *Nature, 457*(7227), 281.

Einthoven, W., & Jolly, W. (1908). The form and magnitude of the electrical response of the eye to stimulation by light at various intensities. *Quarterly Journal of Experimental Physiology, 1*(4), 373–416.

Estévez, O., & Spekreijse, H. (1982). The "silent substitution" method in visual research. *Vision Research, 22*(6), 681–691.

Friedburg, C., Allen, C., Mason, P., & Lamb, T. D. (2004). Contribution of cone photoreceptors and post-receptoral mechanisms to the human photopic electroretinogram. *The Journal of Physiology, 556*(3), 819–834.

Friedburg, C., Thomas, M., & Lamb, T. D. (2001). Time course of the flash response of dark-and light-adapted human rod photoreceptors derived from the electroretinogram. *The Journal of Physiology, 534*(1), 217–242.

Fukuda, Y., Higuchi, S., Yasukouchi, A., & Morita, T. (2012). Distinct responses of cones and melanopsin-expressing retinal ganglion cells in the human electroretinogram. *Journal of Physiological Anthropology, 31*(1), 20.

Gamlin, P. D., McDougal, D. H., Pokorny, J., Smith, V. C., Yau, K. W., & Dacey, D. M. (2007). Human and macaque pupil responses driven by melanopsin-containing retinal ganglion cells. *Vision Research, 47*(7), 946–954.

Gooley, J. J., Mien, I. H., Hilaire, M. A. S., Yeo, S.-C., Chua, E. C.-P., van Reen, E., ... Lockley, S. W. (2012). Melanopsin and rod–cone photoreceptors play different roles in mediating pupillary light responses during exposure to continuous light in humans. *Journal of Neuroscience, 32*(41), 14242–14253.

Granit, R. (1933). The components of the retinal action potential in mammals and their relation to the discharge in the optic nerve. *The Journal of Physiology, 77*(3), 207–239.

Grover, S., Fishman, G. A., Birch, D. G., Locke, K. G., & Rosner, B. (2003). Variability of full-field electroretinogram responses in subjects without diffuse photoreceptor cell disease. *Ophthalmology, 110*(6), 1159–1163.

Grünert, U., Jusuf, P. R., Lee, S., & Nguyen, D. T. (2011). Bipolar input to melanopsin containing ganglion cells in primate retina. *Visual Neuroscience, 28*(01), 39–50.

Güler, A. D., Ecker, J. L., Lall, G. S., Haq, S., Altimus, C. M., Liao, H.-W., ... Zhao, H. (2008). Melanopsin cells are the principal conduits for rod–cone input to non-image-forming vision. *Nature, 453*(7191), 102–105.

Guth, S. L., & Lodge, H. R. (1973). Heterochromatic additivity, foveal spectral sensitivity, and a new color model. *Journal of the Optical Society of America, 63*(4), 450–462.

Heckenlively, J. R., Arden, G. B., Nusinowitz, S., Holder, G. E., & Bach, M. (2006). *Principles and Practice of Clinical Electrophysiology of Vision.* MIT press.

Hood, D. C., Bach, M., Brigell, M., Keating, D., Kondo, M., Lyons, J. S., ... Palmowski-Wolfe, A. M. (2012). ISCEV standard for clinical multifocal electroretinography (mfERG)(2011 edition). *Documenta Ophthalmologica, 124*(1), 1–13.

Horiguchi, H., Winawer, J., Dougherty, R. F., & Wandell, B. A. (2013). Human

trichromacy revisited. *Proceedings of the National Academy of Sciences, 110*(3), E260–E269.
Johnson, E. P., & Bartlett, N. R. (1956). Effect of stimulus duration on electrical responses of the human retina. *Journal of the Optical Society of America, 46*(3), 167–170.
Jusuf, P. R., Lee, S., Hannibal, J., & Grünert, U. (2007). Characterization and synaptic connectivity of melanopsin-containing ganglion cells in the primate retina. *European Journal of Neuroscience, 26*(10), 2906–2921.
Keating, D., Parks, S., Smith, D., & Evans, A. (2002). The multifocal ERG: Unmasked by selective cross-correlation. *Vision Research, 42*(27), 2959–2968.
Kelbsch, C., Strasser, T., Chen, Y., Feigl, B., Gamlin, P. D., Kardon, R., ... Wilhelm, B. J. (2019). Standards in pupillography. *Frontiers in Neurology, 10*, 129.
Liao, H. W., Ren, X., Peterson, B. B., Marshak, D. W., Yau, K. W., Gamlin, P. D., & Dacey, D. M. (2016). Melanopsin-expressing ganglion cells on macaque and human retinas form two morphologically distinct populations. *Journal of Comparative Neurology, 524*(14), 2845–2872.
Lucas, R., Hattar, S., Takao, M., Berson, D., Foster, R., & Yau, K.-W. (2003). Diminished pupillary light reflex at high irradiances in melanopsin-knockout mice. *Science, 299*(5604), 245–247.
McCulloch, D. L., Marmor, M. F., Brigell, M. G., Hamilton, R., Holder, G. E., Tzekov, R., & Bach, M. (2015). ISCEV Standard for full-field clinical electroretinography (2015 update). *Documenta Ophthalmologica, 130*(1), 1–12.
Milosavljevic, N., Cehajic-Kapetanovic, J., Procyk, C. A., & Lucas, R. J. (2016). Chemogenetic activation of melanopsin retinal ganglion cells induces signatures of arousal and/or anxiety in mice. *Current Biology, 26*(17), 2358–2363.
Milosavljevic, N., Storchi, R., Eleftheriou, C. G., Colins, A., Petersen, R. S., & Lucas, R. J. (2018). Photoreceptive retinal ganglion cells control the information rate of the optic nerve. *Proceedings of the National Academy of Sciences, 115*(50), E11817–E11826.
Naka, K., & Rushton, W. (1966). S-potentials from colour units in the retina of fish (Cyprinidae). *The Journal of Physiology, 185*(3), 536–555.
Nasir-Ahmad, S., Lee, S. C., Martin, P. R., & Grünert, U. (2019). Melanopsin-expressing ganglion cells in human retina: morphology, distribution, and synaptic connections. *Journal of Comparative Neurology, 527*(1), 312–327.
Newkirk, G. S., Hoon, M., Wong, R., & Detwiler, P. B. (2013). Inhibitory inputs tune the light response properties of dopaminergic amacrine cells in mouse retina. *Journal of Neurophysiology, 110*(2), 536–552.
Pokorny, J., Jin, Q., & Smith, V. C. (1993). Spectral-luminosity functions, scalar linearity, and chromatic adaptation. *Journal of the Optical Society of America A, 10*(6), 1304–1313.
Prigge, C. L., Yeh, P.-T., Liou, N.-F., Lee, C.-C., You, S.-F., Liu, L.-L., ... Chen, S.-K. (2016). M1 ipRGCs influence visual function through retrograde signaling in the retina. *Journal of Neuroscience, 36*(27), 7184–7197.
Rhudy, M., Bucci, B., Vipperman, J., Allanach, J., & Abraham, B. (2009). *Microphone array analysis methods using cross-correlations. In ASME 2009 International Mechanical Engineering Congress and Exposition.* American Society of Mechanical Engineers281–288.
Schmidt, T. M., Alam, N. M., Chen, S., Kofuji, P., Li, W., Prusky, G. T., & Hattar, S. (2014). A role for melanopsin in alpha retinal ganglion cells and contrast detection. *Neuron, 82*(4), 781–788.
Sieving, P. A., Murayama, K., & Naarendorp, F. (1994). Push–pull model of the primate photopic electroretinogram: A role for hyperpolarizing neurons in shaping the b-wave. *Visual Neuroscience, 11*(3), 519–532.
Smith, V. C., & Pokorny, J. (1975). Spectral sensitivity of the foveal cone photopigments between 400 and 500 nm. *Vision Research, 15*(2), 161–171.
Sonoda, T., Lee, S. K., Birnbaumer, L., & Schmidt, T. M. (2018). Melanopsin phototransduction is repurposed by ipRGC subtypes to shape the function of distinct visual circuits. *Neuron, 99*(4), 754–767 e754.
Spitschan, M., Bock, A. S., Ryan, J., Frazetta, G., Brainard, D. H., & Aguirre, G. K. (2017). The human visual cortex response to melanopsin-directed stimulation is accompanied by distinct visual experience. *Proceedings of the National Academy of Sciences USA, 114*(46), 12291–12296.
Swanson, W. H., Ueno, T., Smith, V. C., & Pokorny, J. (1987). Temporal modulation sensitivity and pulse-detection thresholds for chromatic and luminance perturbations. *Journal of the Optical Society of America A, 4*(10), 1992–2005.
Viney, T. J., Balint, K., Hillier, D., Siegert, S., Boldogkoi, Z., Enquist, L. W., ... Roska, B. (2007). Local retinal circuits of melanopsin-containing ganglion cells identified by transsynaptic viral tracing. *Current Biology, 17*(11), 981–988.
Vugler, A. A., Redgrave, P., Lawrence, J., Greenwood, J., & Coffey, P. J. (2007). Dopamine neurones form a discrete plexus with melanopsin cells in normal and degenerating retina. *Experimental Neurology, 205*(1), 26–35.
Wong, K. Y., Dunn, F. A., Graham, D. M., & Berson, D. M. (2007). Synaptic influences on rat ganglion-cell photoreceptors. *The Journal of Physiology, 582*(1), 279–296.
Zele, A. J., Adhikari, P., Cao, D., & Feigl, B. (2019a). Melanopsin and cone photoreceptor inputs to the afferent pupil light response. *Frontiers in Neurology, 10*, 529.
Zele, A. J., Adhikari, P., Cao, D., & Feigl, B. (2019b). Melanopsin driven enhancement of cone-mediated visual processing. *Vision Research, 160*, 72–81.
Zele, A. J., Adhikari, P., Feigl, B., & Cao, D. (2018). Cone and melanopsin contributions to human brightness estimation. *Journal of the Optical Society of America A, 35*(4), B19–B25.
Zele, A. J., Feigl, B., Adhikari, P., Maynard, M. L., & Cao, D. (2018). Melanopsin photoreception contributes to human visual detection, temporal and colour processing. *Scientific Reports, 8*(1), 3842.
Zele, A. J., Feigl, B., Kambhampati, P. K., Aher, A., McKeefry, D., Parry, N., ... Kremers, J. (2017). A Temporal White Noise Analysis for Extracting the Impulse Response Function of the Human Electroretinogram. *Translational Vision Science & Technology, 6*(6) 1 1.
Zele, A. J., Feigl, B., Kambhampati, P. K., Hathibelagal, A. R., & Kremers, J. (2015). A method for estimating intrinsic noise in electroretinographic (ERG) signals. *Documenta Ophthalmologica, 131*(2), 85–94.
Zhang, D.-Q., Belenky, M. A., Sollars, P. J., Pickard, G. E., & McMahon, D. G. (2012). Melanopsin mediates retrograde visual signaling in the retina. *PloS ONE, 7*(8), e42647.
Zhang, D.-Q., Wong, K. Y., Sollars, P. J., Berson, D. M., Pickard, G. E., & McMahon, D. G. (2008). Intraretinal signaling by ganglion cell photoreceptors to dopaminergic amacrine neurons. *Proceedings of the National Academy of Sciences, 105*(37), 14181–14186.
Zhao, X., Pack, W., Khan, N. W., & Wong, K. Y. (2016). Prolonged inner retinal photoreception depends on the visual retinoid cycle. *Journal of Neuroscience, 36*(15), 4209–4217.